Supporting Information for

Dynamic Crossover in Metallic Glass Nanoparticles

Shan Zhang (张珊) [1], Weihua Wang (汪卫华) [2], Pengfei Guan (管鹏飞) [1]

[1] *Beijing computational science research center, Beijing 100193, China*

[2] *Chinese Academy of Sciences, Institute of Physics, Beijing 100190, China*

1 The calculated self-intermediate scattering functions (SISF)

SISFs for $Cu_{50}Zr_{50}$ system. We have calculated the SISF of $Cu_{50}Zr_{50}$ metallic glass nanoparticles (MGNs, with the size of 0.8, 1.0, 1.3, 1.5, 3.0 nm) and bulk MG. With the size increases, the relaxation dynamics become slower.

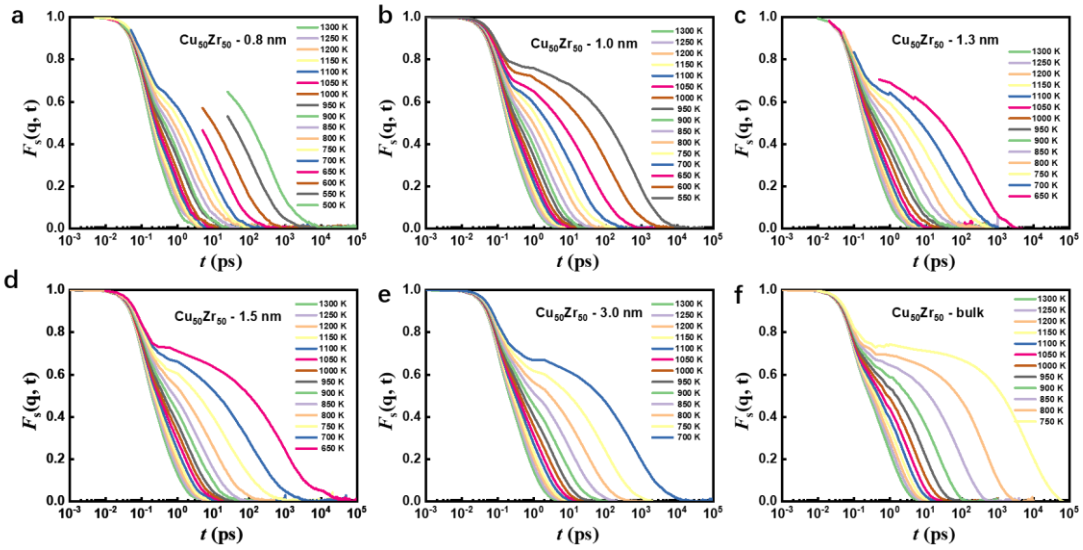

Fig.S1. The SISFs of $Cu_{50}Zr_{50}$ MGNs and bulk MG with various sizes at the different temperatures.

SISFs for $Cu_{86}Zr_{14}$ MGNs. We have calculated the SISF of $Cu_{86}Zr_{14}$ MGNs (with the size of 0.8, 1.0, 1.3, 1.5, 3.0 nm) and bulk MG. The trend is consistent with the $Cu_{50}Zr_{50}$ system.

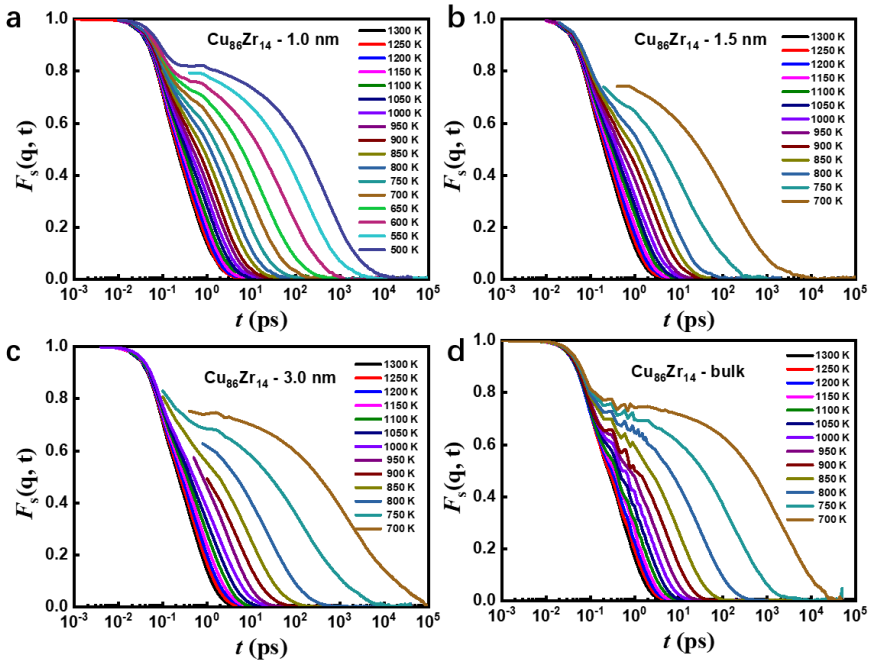

Fig.S2. The SISFs of $Cu_{86}Zr_{14}$ MGNs and bulk MG with various sizes at the different temperatures.

2 The Angell plots and normalized fragility index for $Cu_{86}Zr_{14}$ system

We plotted the Angell plots of the $Cu_{86}Zr_{14}$ system and observed the fragile-to-strong transition of dynamics. The critical size D_c is ~1.5 nm which indicates the composition-independent crossover behaviors of kinetic fragility.

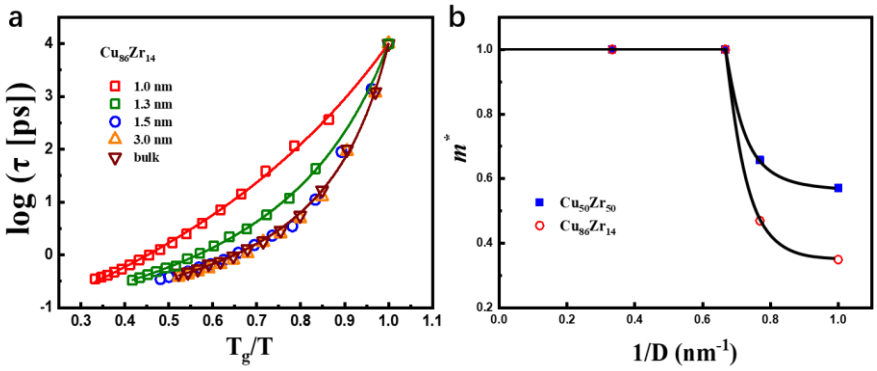

Fig. S3. (a) The Angell plots of relaxation time τ_α versus T_g/T in $Cu_{86}Zr_{14}$ system; (b) the normalized fragility index m* with 1/D for $Cu_{86}Zr_{14}$ and $Cu_{50}Zr_{50}$ systems.

3 The shell-dependent dynamics for the $Cu_{50}Zr_{50}$ system

The core-shell feature of MGNs. The core-shell feature is significant in the atomic configurations of MGNs. We defined the outermost shell as the surface shell and the rest part as the inner shells.

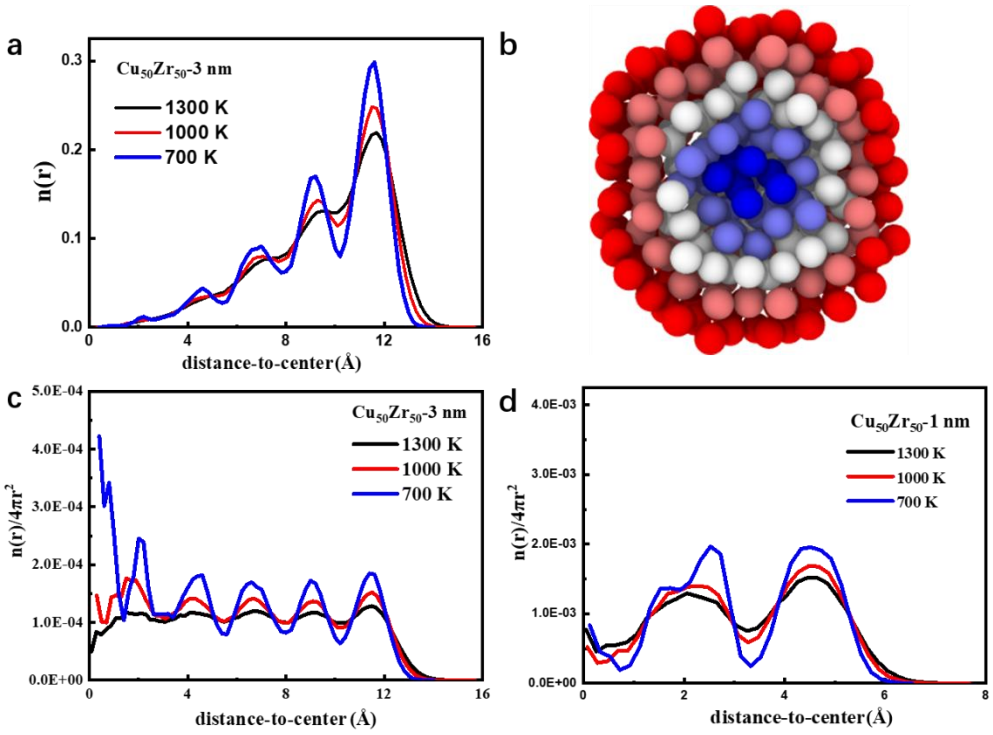

Fig. S4. (a) The number of atoms against the distance to the center at 700 K, 1000 K, and 1300 K for the 3.0 nm $Cu_{50}Zr_{50}$ systems. (b) The visualization diagram of the 3.0 nm $Cu_{50}Zr_{50}$ system with colored shells. (c) and (d) The number density in each shell at 700 K, 1000 K, and 1300 K for 3.0 nm and 1.0 nm $Cu_{50}Zr_{50}$ systems, respectively.

The element distribution in the surface shell. The surface mobility played an essential role in the dynamics of MGNs. We analyzed the atomic percent of Cu element in the surface shell of various MGNs (averaged 100 samples to reduce statistical errors). As shown in Fig. S5, there is no segregation of chemical components on the surface.

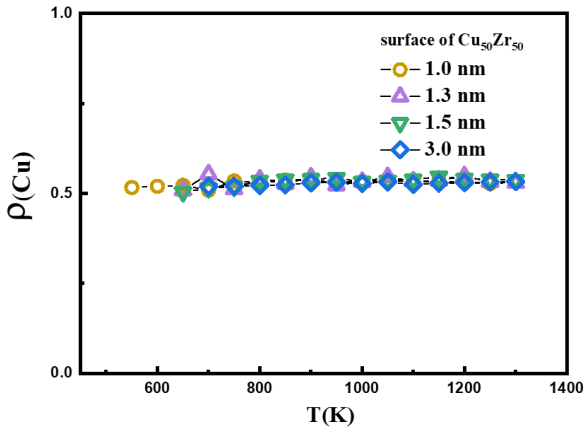

Fig. S5. The atomic percent of Cu element in the surface shell of $Cu_{50}Zr_{50}$ MGNs.

Shell-dependent relaxation dynamics. To examine shell-dependent dynamics in MGNs, we defined the SISF of various shells as:

$$F_{s,L}(Q,t) = \frac{1}{N}\langle \sum_{l=1}^{N} exp\{-iQ \cdot [r_l(t,L) - r_l(0,L)]\}\rangle \quad (1)$$

where N is the number of particles in the L-shell and $r_l(t,L)$ and $r_l(0,L)$ are the position of the atom in the L-shell at 0 and t time simultaneously. We plotted the SISFs of the surface shell and inner shells in 1.0 nm and 3.0 nm MGNs in Fig. S6. The surface relaxation time $\tau_{\alpha,s}$ as a function of temperature are shown in Fig. S7. The surface dynamics of MGNs are faster than the inner-shells. [1]

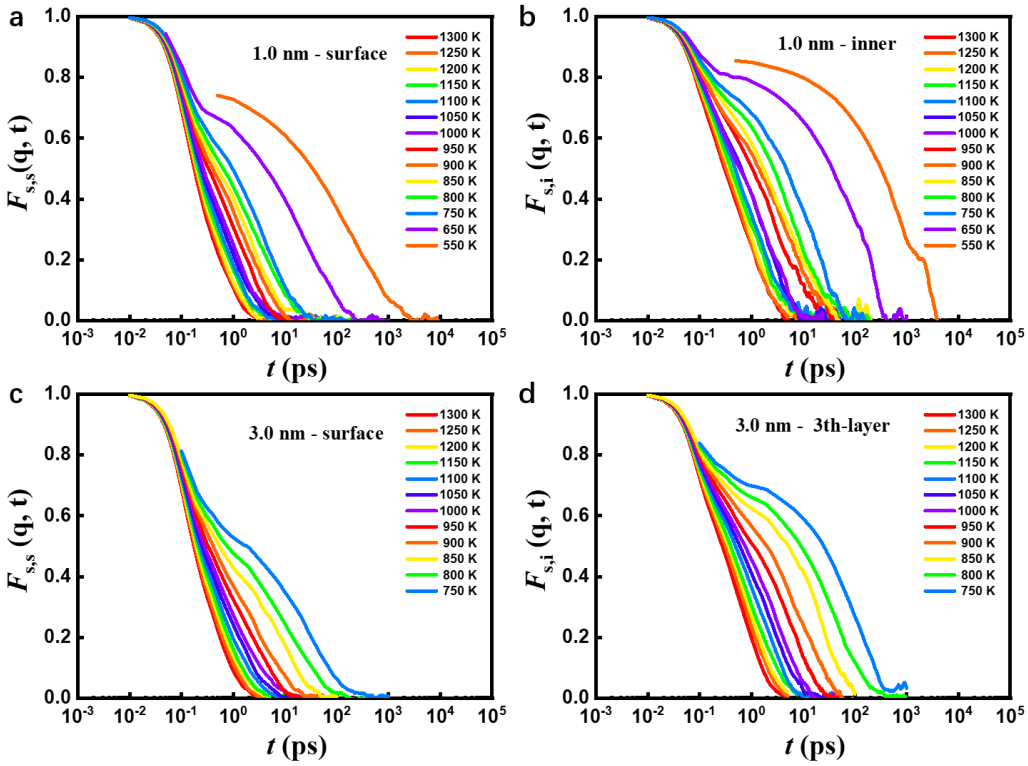

Fig. S6. The shell-dependent SISF of the 1.0 nm and 3.0 nm $Cu_{50}Zr_{50}$ MGNs at the different temperatures.

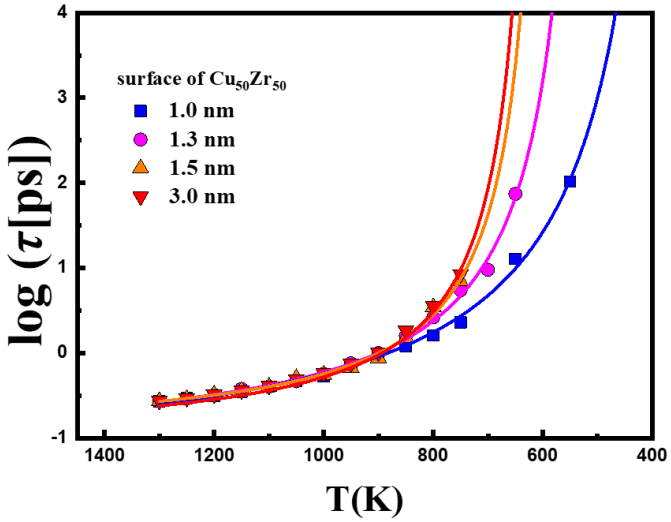

Fig. S7. The surface relaxation time $\tau_{\alpha,s}$ versus T of $Cu_{50}Zr_{50}$ MGNs. The solid curves are the VFT fitting curves.

4 E_A spectra and the effective barrier $\overline{E}_A$

E_A spectra. We employed CG algorithm to prepare the inherent structure of MGNs which is quenched from different parent temperatures instantaneously. To obtain the E_A spectrum, we applied 50 ~500 activation-relaxation technique (ART) searches for each group of atoms. We set the initial perturbation displacement of 0.5 Å and the direction of perturbation randomly in the searching events. The perturbation radius is 3.2 Å. And the force threshold is below 0.05 eV/Å. Thus, we could get the raw data by 25,000 ART searches for a given sample with 1nm and 3 nm at 600 K, 750 K, 900 K, 1050 K, and 1300 K. We should use two removal steps[2, 3] to obtain ~ 2,000 effective searches (in different samples, the number will be different). Finally, we can get the E_A spectrum for each sample. Because the temperature is up the glass transition temperature, we selected 5 and 10 configurations at each temperature for a statistical average. Figure S8 (a) shows the E_A spectra of MGNs with different sizes. With the size increasing, the distribution of activation energy has a broader range. In Fig. S9, we plotted the 1.0 nm and 3.0 nm samples' E_A spectra at various temperatures.

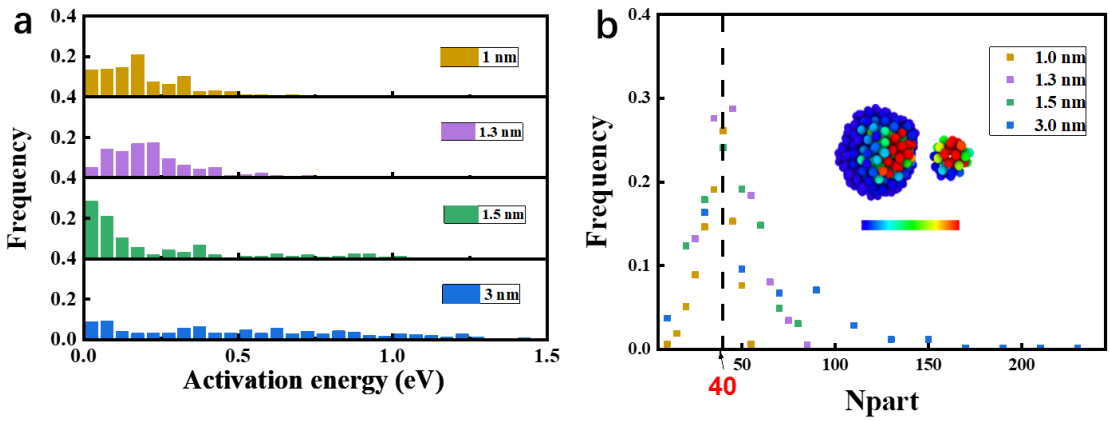

Fig. S8 (a) E_A spectra of 1.0 nm, 1.3 nm, 1.5 nm, and 3.0 nm $Cu_{50}Zr_{50}$ MGNs at 750 K. (b) Distribution of the number of atoms participating in activation event. The inset shows the distribution of atoms when the number of active atoms is ~40.

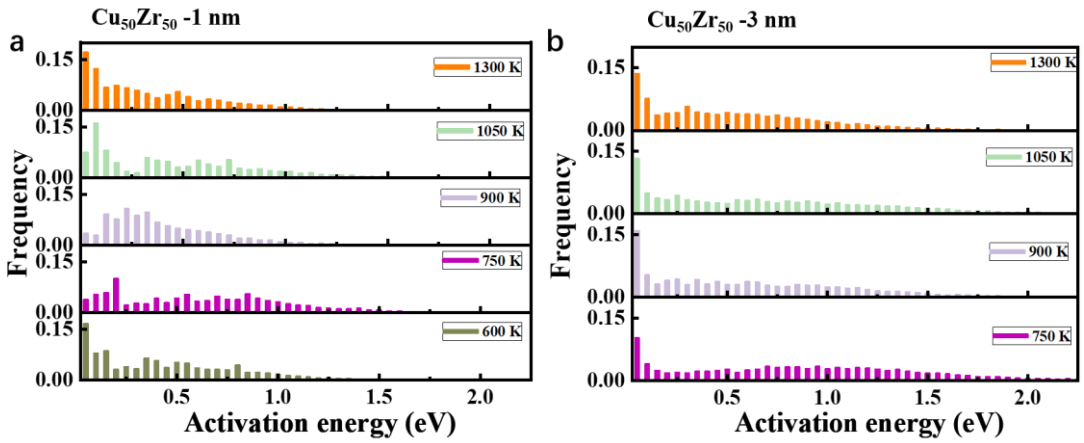

Fig. S9. E_A spectra of (a) 1.0 nm and (b) 3.0 nm $Cu_{50}Zr_{50}$ MGNs with various parent temperatures.

The arithmetic mean E_A, $\bar{E}_{A,k}$ and Effective barrier $\bar{E}_A$ The arithmetic mean of each atom's E_A, $\bar{E}_{A,k}$ is the arithmetic mean of all effective searches' activation energy E_A of k atom. It was calculated by Eq. (2)

$$\bar{E}_{A,k} = \frac{1}{N_{event\ ,k}} \sum_{i=1}^{N_{event\ ,k}} E_A(i,k) \tag{2}$$

where $E_A(i,k)$ is the k atom's activation energy in i^{th} event. $N_{event\ ,k}$ is the number of the effective events of k atom. The effective barrier was calculated by Eq. (3)[4] to keep high energy barriers dominate the diffusivity.

$$\bar{E}_A(E_{IS,T}) = k_B T \cdot \ln\left[\int P(E_A|E_{IS}) e^{\frac{E_A}{k_B T}} dE_A\right] \tag{3}$$

References

1. Chen N, Wang D, Guan P F, Bai H Y, Wang W H, Zhang Z J, Hahn H, & Gleiter H 2019 *Appl. Phys. Lett.* **114**.
2. Zhang S, Liu C, Fan Y, Yang Y, & Guan P 2020 *J. Phys. Chem. Lett.* **11** 2781.
3. Fan Y, Iwashita T, & Egami T 2014 *Nat. Commun.* **5**.
4. Wang Y-J, Du J-P, Shinzato S, Dai L-H, & Ogata S 2018 *Acta Mater.* **157** 165.